JOC The Journal of Organic Chemistry

Article

pubs.acs.org/joc

Absolute Configuration Assignment of Chiral Resorcin[4]arenes from ECD Spectra

Gerardo Concilio,[†] Carmen Talotta,[†] Carmine Gaeta,[†] Placido Neri,*[,†] Guglielmo Monaco,*[,†] Riccardo Zanasi,[†] Daniele Tedesco,*[,‡] and Carlo Bertucci[‡]

[†]Department of Chemistry and Biology "A. Zambelli", University of Salerno, Via Giovanni Paolo II, 132, Fisciano 84084 SA, Italy

[‡]Department of Pharmacy and Biotechnology, University of Bologna, Via Belmeloro, 6, Bologna 40126, Italy

Supporting Information

ABSTRACT: Racemates of five chiral resorcin[4]arenes, four tetra-*O*-substituted and one hepta-*O*-substituted, have been resolved by enantioselective HPLC, and their ECD spectra have been recorded online by stopped-flow measurements. The absolute configuration has been assigned by comparison of the experimental ECD spectra with DFT and semiempirical calculations. For the four tetra-*O*-substituted resorcin[4]-arenes, the ECD exciton couplet at longer wavelength depends on the chirality induced in the arene scaffold by the substituents rather than on the precise nature of the substituents themselves. Accordingly, the exciton chirality model with excitons localized on the arene scaffold, here generalized to C_n symmetry, accurately describes the relationship between stereochemistry and chiroptical properties for this couplet, while its application at shorter wavelengths is unsafe. For the significantly larger hepta-*O*-substituted system the assignment particularly benefits from the use of the semiempirical ZINDO method.

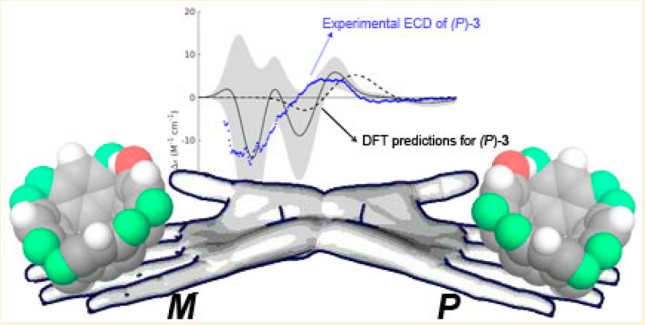

INTRODUCTION

Among the bowl-shaped macrocycles,[1] resorcin[4]arenes[2] play a prominent role in supramolecular chemistry in the synthesis of cavitands,[3] carcerands,[2] and self-assembled capsules.[4] A particular emphasis has been also devoted to chiral bowl-shaped macrocycles such as chiral resorcin[4]arenes and calix[4]arenes, which can be synthesized by appending chiral substituents to the macrocyclic skeleton or by generation of a dissymmetric pattern with achiral substituents,[5] leading to the so-called inherent chirality.[6,7]

In the last decades, numerous examples of chiral resorcin[4]-arenes have been reported[7] and their supramolecular properties such as self-assembly and self-sorting have been studied.[8] The use of these compounds as supramolecular chiral building blocks requires their resolution and the identification of their absolute configuration (AC), which can be determined by use of chiroptical spectroscopies, especially thanks to the advancement of computational techniques.[9,10]

In this framework, a racemate of an inherently chiral calix[4]arene derivative has been recently synthesized and resolved.[11,12] The absolute stereochemistry of its enantiomers was assigned by comparison between the experimental chiroptical properties in solution and the results of density functional theory (DFT) calculations.[12] From an analytical point of view, the stereochemical characterization was achieved after resolution of the racemic mixture by preparative enantioselective high-performance liquid chromatography (eHPLC) followed by off-line optical rotatory dispersion (ORD) and electronic circular dichroism (ECD) spectroscopic analysis on the two collected enantiomeric fractions. As an extension of that work, the present investigation will focus on the determination of the AC of five *O*-functionalized resorcin[4]arenes, which have been synthesized by weak-base-promoted *O*-alkylation of *C*-undecylresorcin[4]arene.[13] The AC will be assessed by comparison between their experimental ECD spectra and those determined by DFT and semiempirical calculations; an interpretation of the results in terms of the exciton chirality model (ECM) will also be given. As a convenient alternative to the analytical method previously used, the hyphenation of eHPLC with a circular dichroism detector (eHPLC−CD) will be adopted. This allows the online measurement of ECD spectra in stopped-flow mode for each enantiomeric fraction.[14,15]

The structures of the five resorcin[4]arenes under investigation are reported in Scheme 1. Due to the presence of the undecyl chains on the methine bridges of the resorcin[4]arene scaffold, any substitution pattern on the upper rim incompatible with a vertical symmetry plane generates four stereogenic centers, whose AC is given for both enantiomers of all compounds in Scheme 1. As an alternative to the usual *R*/*S* notation, the close similarity of resorcin[4]arenes with inherently chiral calix[4]arenes has led to the preference of the *P*/*M* notation for axial chirality[16] in the stereochemical

Received: September 26, 2016
Published: December 7, 2016

DOI: 10.1021/acs.joc.6b02349
J. Org. Chem. 2017, 82, 202−210

Scheme 1. Structures of the Chiral Resorcin[4]arenes under Investigation

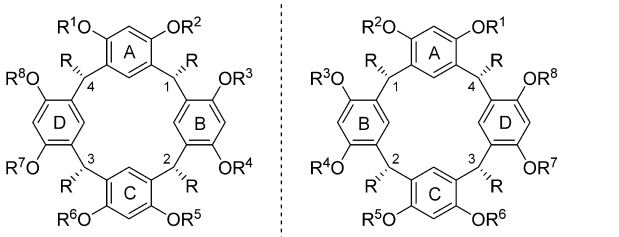

(*P*) = (*P*,*P*,*P*,*P*) = (1*S*,2*S*,3*S*,4*S*)	**1a, 1b**	(1*R*,2*R*,3*R*,4*R*) = (*M*,*M*,*M*,*M*) = (*M*)
(*M*) = (*0*,*M*,*M*,*0*) = (1*R*,2*R*,3*R*,4*S*)	**2a, 2b**	(1*S*,2*S*,3*S*,4*R*) = (*0*,*P*,*P*,*0*) = (*P*)
(*P*) = (*0*,*0*,*0*,*P*) = (1*S*,2*R*,3*R*,4*S*)	**3**	(1*R*,2*S*,3*S*,4*R*) = (*0*,*0*,*0*,*M*) = (*M*)

R = *n*-$C_{11}H_{23}$

1a	$R^{1,3,5,7}$ = -CH_3	$R^{2,4,6,8}$ = -H
1b	$R^{1,3,5,7}$ = -CH_2Ph	$R^{2,4,6,8}$ = -H
2a	$R^{1,2,4,6}$ = -CH_3	$R^{3,5,7,8}$ = -H
2b	$R^{1,2,4,6}$ = -CH_2Ph	$R^{3,5,7,8}$ = -H
3	R^{1-7} = -COPh	R^{8} = -H

description of both classes of compounds,[7,17] where the AC is labeled *P* or *M* if the priorities of the resorcinol substituents decrease in clockwise or anticlockwise direction when viewed from a position above the polar rim. However, the compact *P*/*M* notation can only be applied without complications to C_4-symmetric resorcinarenes:[5] for resorcinarenes of lower symmetry the relative priority of the resorcinol substituents can differ for each of the rings A−D, ending up with a four-letter stereochemical code (a *P* or *M* letter for each ring), with no advantage in compactness over the standard *R*/*S* notation. This is not the case for the patterns of substitution considered here, where the two substituents, e.g., OR_1 and OR_2 for ring A, are either the same (e.g., $R_1 = R_2$, and ring A is then assigned a 0 code of axial chirality) or have the same relative priority (e.g., $R_3 < R_4$, and $R_5 < R_6$, leading to the same axial chirality for rings B and C), ending up with a single non-null letter code *P* or *M*, which can then be conveniently used as a shorthand (Scheme 1). Derivatives **1a**,**b**, **2a**,**b**, and **3** are representative of three groups with different capabilities to form hydrogen bonds (HBs), which are the structural elements which most affect the conformational properties of resorcin[4]arenes.[18] The compounds with a 1,3,5,7-*O*-substitution pattern (**1a**,**b**) can occur as C_4-symmetric crown conformers with 4 symmetry-equivalent HBs, while the C_1-symmetric compounds with a 1,2,4,6-*O*-substitution pattern (**2a**,**b**) can still form four HBs, but those bonds are not related by rotational symmetry, and a nonsymmetric pinched crown conformation is expected.[19] The two possible pinched crowns will be labeled **A** and **B** according to Scheme 2. Finally, the nonsymmetric hepta-*O*-substituted derivative (**3**) can form at most a single HB, which is insufficient to favor the sterically destabilized crown conformation,[18] and a boat conformation is expected. The two possible boat conformations will be labeled **A** and **B** according to Scheme 2. The modeling of tetra-*O*-substituted resorcin[4]arenes can thus be anticipated to be easier than that of compound **3** on the grounds of a smaller conformational space. Within tetra-*O*-substituted derivatives, the interpretation of the ECD spectra for compounds **1a** and **2a** should be still easier than for compounds **1b** and **2b** because methyl groups are less efficient chromophores compared to benzyl groups.

RESULTS AND DISCUSSION

Enantioselective eHPLC−CD Analysis. A preliminary eHPLC optimization study allowed the identification of the best chromatographic conditions for the enantioresolution of

Scheme 2. Crown Conformation and the Two Possible Pinched-Crown and Boat Conformations of the Resorcin[4]arenes[a]

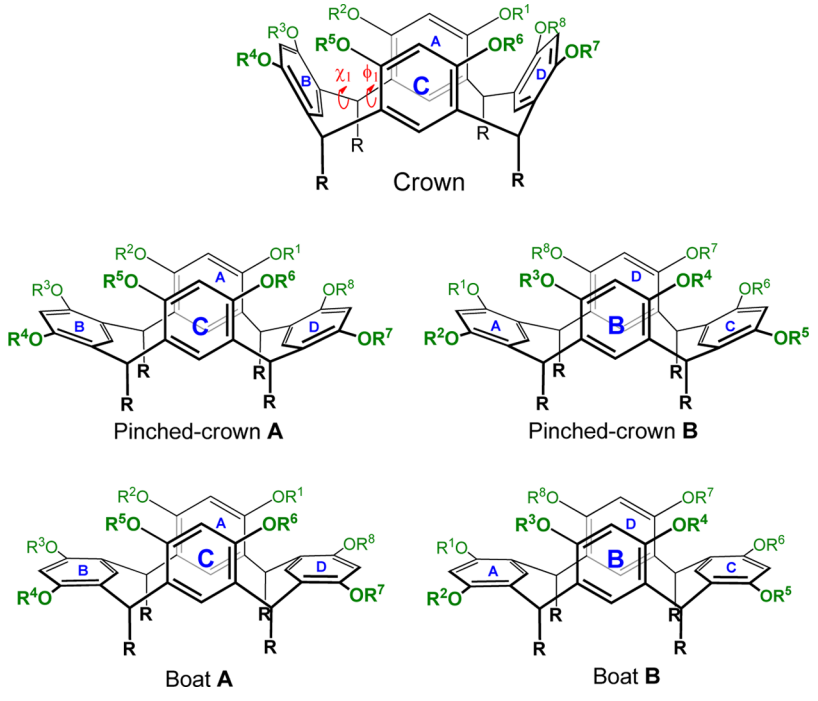

[a]The definition of the substituents is as in Scheme 1. The pair of dihedral angles ϕ_1 and χ_1 (and the other three pairs centered on the other three methines) are defined in terms of the C atoms of the larger macrocycle.[20]

DOI: 10.1021/acs.joc.6b02349
J. Org. Chem. 2017, 82, 202−210

resorcin[4]arenes, which are reported in Table 1; satisfactory values of enantioselectivity and resolution were obtained for all analyzed compounds. Detailed results of the optimization study for the enantioresolution of compounds **2b** and **3** are reported in the Supporting Information (Tables S1–S2).

Table 1. Optimized Chromatographic Conditions and Corresponding Parameters for the eHPLC Enantioresolution of Resorcin[4]arenes 1–3[a]

	column	mobile phase	k_1	α	R_S	EO
1a	Chiralpak AD	HEX/IPA 99:1 (v/v), 1 mL min^{-1}	1.08	1.45	1.66	+,–
1b	Chiralpak AD	HEX/IPA 99:1 (v/v), 1 mL min^{-1}	4.95	1.34	1.51	+,–
2a	Chiralpak AD	HEX/IPA 97:3 (v/v), 1 mL min^{-1}	1.75	1.76	2.73	+,–
2b	Amylose-2	HEX/MET 96:4 (v/v), 1 mL min^{-1}	1.50	1.19	1.52	–,+
3	Cellulose-1	HEX/IPA 97:3 (v/v), 1 mL min^{-1}	2.72	1.40	1.48	–,+

[a]Key: k_1, capacity factor for the first-eluted enantiomeric fraction; α, enantioselectivity; R_S, resolution; EO, elution order based on the sign of $\Delta\varepsilon$ at 300 nm (for **1a**, **1b**, **2a**, and **2b**) or 275 nm (for **3**); HEX, *n*-hexane; IPA, 2-propanol; MET, methanol.

The subsequent determination of the ECD spectra for the enantiomers of the resorcin[4]arenes under investigation was carried out following a stopped-flow eHPLC–CD approach. All recorded spectra (Figures S1 and S2) display an excellent signal-to-noise ratio and limited baseline drift even at shorter wavelengths.

The UV spectra of tetra-*O*-substituted resorcin[4]arenes display similar intensities (Figure S3), while ECD spectra show interestingly regular features (Figure 1). A completely different behavior, on the other hand, is displayed by the hepta-*O*-benzoyl derivative **3**, whose electronic properties are extensively influenced by the contribution of benzoyl substituents (Figure 2 and Figure S4).

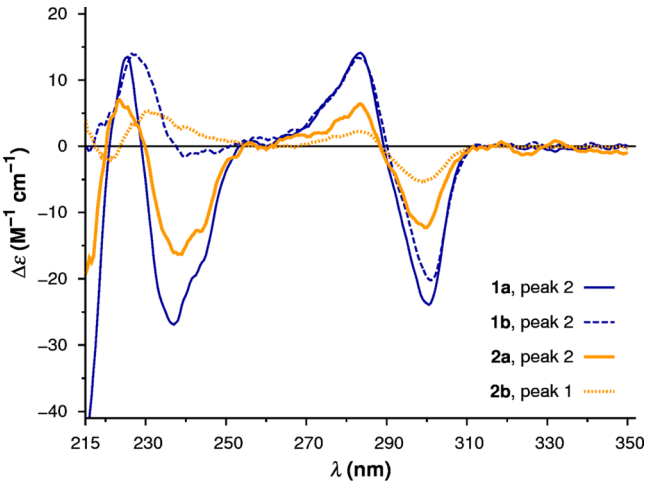

Figure 1. Experimental ECD spectra of the enantiomeric fractions of compounds **1a**,**b** and **2a**,**b** displaying a negative exciton couplet for the aromatic ^1L_b transitions (310–270 nm). Spectra were acquired in stopped-flow mode during the eHPLC–CD enantioresolution of the corresponding racemic mixture; solvents for the measurements correspond to the mobile-phase compositions reported in Table 1.

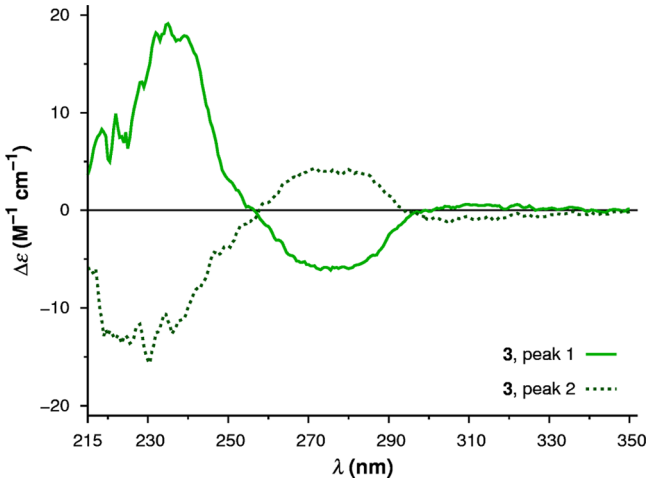

Figure 2. Experimental ECD spectra of the enantiomeric fractions of compound **3**. Spectra were acquired in stopped-flow mode during the eHPLC–CD enantioresolution of the racemic mixture; the solvent for the measurements corresponds to the mobile phase composition reported in Table 1.

The 1,3,5,7-*O*-substitution pattern generates an ECD exciton couplet centered at the absorption maximum of the aromatic ^1L_b transitions,[21] which has the same magnitude irrespective of the nature of substituents (benzyl or methyl groups). The exciton is therefore due to the coupling between the resorcinol rings of the resorcin[4]arene skeleton, whose ^1L_b transition moments are oriented along the same direction by the regular *O*-substitution pattern. The 1,2,4,6-*O*-substitution pattern still generates an ECD exciton couplet centered at the absorption maximum of the aromatic ^1L_b transitions, but the magnitude differs depending on the nature of substituents. The ECD couplet of the tetra-*O*-benzyl derivative **2b** has a lower intensity than the corresponding tetra-*O*-methyl derivative **2a**, indicating that the coupling between resorcinol rings is probably affected by the double *O*-substitution of one resorcinol ring.

The more effective coupling between resorcinol rings with a regular *O*-substitution pattern is confirmed by the comparison between the ECD profiles of tetra-*O*-methyl derivatives: the intensity is higher for the regular 1,3,5,7-*O*-substitution pattern (**1a**) than for the irregular 1,2,4,6-*O*-substitution pattern (**2a**) throughout the spectral range of analysis. A similar behavior is observed for the tetra-*O*-benzyl derivatives **1b** and **2b**, but their high-energy ECD spectra are significantly more affected by the contribution of aromatic substituents.

AC Determination through DFT Calculations. The computation of the ECD spectra of the studied compounds is challenging in consideration of their dimension, especially for **3**, and of the fact that they are flexible systems. However, the presence of intramolecular HBs can reduce significantly the relevant conformational space, especially for systems **1a**,**b** and **2a**,**b**, where up to four HBs can be formed, and the crown conformation of the resorcin[4]arene scaffold should be stabilized.[18] For these systems, we modeled therefore conformers with four well-formed HBs for an arbitrarily chosen *M* stereochemistry. The pendant groups (Me and CH_2Ph) have been initially set in the plane of the aromatic ring (an orientation that minimizes the MMFF energy of monomeric units), and the geometries have been optimized at the B3LYP/6-31G* level (Figures S4–S8). The crown conformations are preserved in the optimizations, although the conformations of

DOI: 10.1021/acs.joc.6b02349
J. Org. Chem. 2017, 82, 202–210

2a,**b** are better described as pinched-crowns **B**, as can be inferred from the different values of either the ϕ_i and χ_i angles[20] (Scheme 2) or the inclination angles Φ_i of the aromatic rings (Table 2).

Table 2. Conformational Features of the B3LYP/6-31G*-Optimized Conformers Used for the ab Initio Calculations of the ECD Spectra of Figure 3[a]

	rings	ϕ (deg)	χ (deg)	Φ (deg)
(*M*)-**1a**	A–B	−92.9	93.8	41.3
	B–C	−92.9	93.8	41.3
	C–D	−92.9	93.8	41.3
	D–A	−92.9	93.8	41.3
(*M*)-**1b**	A–B	−92.6	94.1	41.6
	B–C	−92.6	94.1	41.6
	C–D	−92.6	94.1	41.6
	D–A	−92.6	94.1	41.6
(*M*)-**2a**	A–B	101.5	−84.9	38.3
	B–C	85.9	−101.0	21.1
	C–D	101.5	−82.2	41.4
	D–A	83.0	−102.5	17.9
(*M*)-**2b**	A–B	102.8	−82.5	52.2
	B–C	85.0	−103.5	29.7
	C–D	103.5	−77.8	52.5
	D–A	79.2	−104.7	23.8

[a]The angle Φ_i (i = A, B, C, D) increases from 0° to 90° while bending the upright i-th ring of the resorcin[4]arene towards the plane of the methine bridges (see the Computational Methods for its definition).

These structures for compounds **1a**,**b** and **2a**,**b** have been used for the computation of ECD spectra by time-dependent density functional theory (TDDFT) at the substantially robust[22] B3LYP/6-31++G* and PBE0/6-31++G* levels (Figure 3). As compared to the B3LYP calculations, the PBE0 calculations give more intense peaks shifted some 10 nm toward the blue, but overall, the two methods give qualitatively similar results (in these calculations the basis set is large enough that length and velocity formalisms give substantially identical results). For all four compounds, the negative ECD couplets in the long-wavelength region of the enantiomeric fractions shown in Figure 1 are reasonably reproduced, particularly so for the B3LYP calculations (the positive part of the computed couplet is actually very small in the case of **2a**). On these grounds, the AC of (*M*)-isomers in Scheme 1 can be associated with the experimental ECD spectra of the enantiomeric fractions of **1a**,**b** and **2a**,**b** plotted in Figures 1 and 3. The computed negative couplets for (*M*)-isomers are fully consistent with the computed positive couplets already reported for C_4 resorcin[4]-arenes of (*P*) configuration which differs only marginally from (*P*)-**1a**.[23b,24] The AC of one of those resorcin[4]arenes was also determined by X-ray diffraction,[23a] a fact that gives further credit to the ECD analysis.

Interestingly, these single-conformer calculations are also in reasonable agreement at shorter wavelengths in the case of **1a** and **2a**, where the pendants are not chromophores. On the other hand, when the pendants are chromophores (**1b** and **2b**), the shorter wavelength portion of the computed spectra disagrees qualitatively with the experimental spectra. This failure could be due to the influence of different conformations of the pendants and/or to an insufficient level of the computational method used. As for the latter possibility, a clear limitation is the number of excited states: according to our

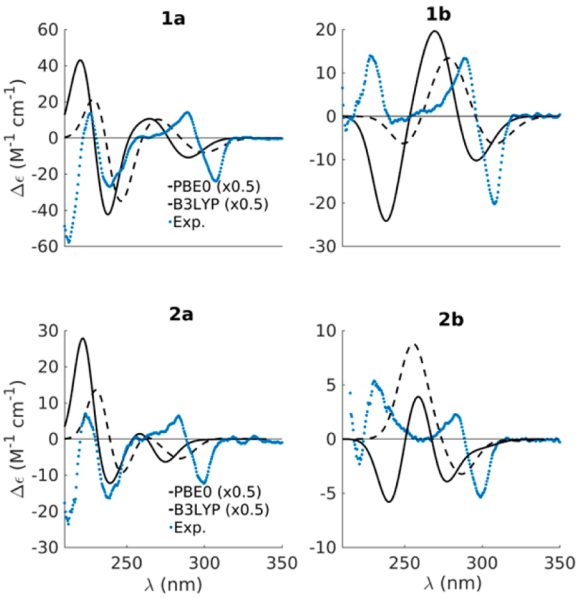

Figure 3. Comparison of experimental and computed ECD spectra for compounds **1a**,**b** and **2a**,**b**. Experimental spectra are drawn as blue-dotted lines and correspond to the enantiomeric fractions shown in Figure 1; TDDFT spectra for (*M*)-isomers, unshifted but multiplied by a factor 0.5, are drawn in continuous or dashed lines for PBE0/6-31++G* and B3LYP/6-31++G* levels, respectively. See the text for details of the single-conformer TDDFT calculations.

method of calculation, the highest energy transition falls close to the border of the experimental spectral range for **1a** and **2a** (225.69 and 218.98 nm, respectively), but it is further away for **1b** and **2b** (245.48 and 240.00 nm, respectively). Indeed, as these compounds are richer in chromophores, they have a denser virtual space and require a greater number of excited states to be properly described. As an alternative to the needed increase of the number of excited states, which leads to a significantly longer computation time, we have attempted the adoption of a lower level of computation, with a less dense virtual space. In addition to the coverage of a wider spectral range with the same number of states, a lower level method can also allow investigating the role of conformations with significantly reduced computational cost. We then adopted the semiempirical ZINDO method.[25] In order to consider the effect of conformations, the pendants have been thoroughly rotated and the energy of the resulting conformers has been optimized at the B3LYP/6-31G* level. Although the ZINDO method leads to rather good results, it shares the difficulties of calculations with small basis sets: it is plagued by the gauge origin problem; i.e., it generally leads to unphysical differences of spectra computed in the length and velocity formalism. We then computed the mean of the spectra resulting from the two formalisms, and we have reported the range covered by the two computations at the Boltzmann-averaged ZINDO//B3LYP/6-31G* level (Figure 4, panels I). As can be seen, although the signs themselves of the small peaks around 260 nm are not strictly determined, the overall shapes of the ECD spectra are unchanged in the two formalisms. We have then figured out the relevance of the higher energy conformations shading the region of a single standard deviation around the Boltzmann-averaged spectra computed from the conformations with a population larger than 0.01. For **1b**, high energy conformational freedom changes the relative intensity of the peaks, but not

DOI: 10.1021/acs.joc.6b02349
J. Org. Chem. 2017, 82, 202–210

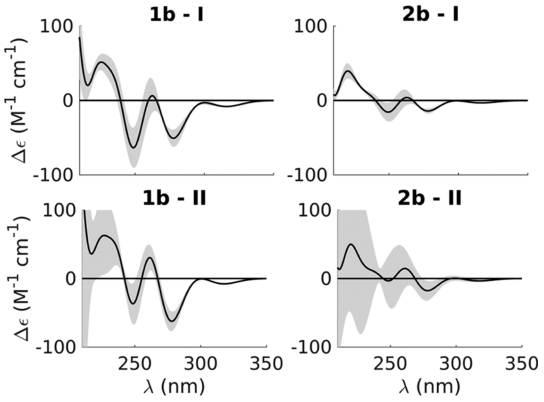

Figure 4. Conformational averaged ECD spectra computed at the ZINDO//B3LYP/6-31G* level for (*M*)-**1b** and (*M*)-**2b**. In the top panels (I), the shaded area is limited by the spectra computed by the length and velocity formalisms, while the black line corresponds to the mean of the spectra. In the bottom panels (II), the black line is ECD spectrum (length formalism) Boltzmann-averaged over the low energy conformers; the standard deviations of the molar circular dichroism over the low energy conformers have been used to draw the shaded region.

their signs. For **2b** instead, the conformational freedom changes significantly the overall shape of the spectrum. Notably the Boltzmann-averaged spectra have the same appearance of the experimental spectra (Figure 1). The assignment of the AC for **1b** and **2b**, already advanced from the longer wavelength couplet, is then further confirmed by the short wavelength portion of the spectra.

A "scaffold-based" ECD spectrum, like the ones discussed above, cannot be expected for **3**. Indeed, this species cannot adopt the compact crown conformation, due to the possibility to form at most a single HB and due to the bulkiness of the seven benzoyl groups. Moreover, the ECD spectrum will be strongly affected by the orientation of the benzoyl groups, which are excellent chromophores. In addition, the ability of a single HB to reduce the relevant conformational space, as happened for **1a**, **1b**, **2a**, and **2b**, could be questioned and deserves discussion. Of the two possible boat conformations of **3** (Scheme 2), **A** has the phenolic ring D bent toward the methine carbon atoms; **B** has that ring upright. As a difference with **1a**,**b** and **2a**,**b**, the HB between the phenolic hydroxyl group and the adjacent ring can now form in two ways: either with the aryloxy or with the carbonyl oxygen of the ester group. Conformations with an H-bond to the adjacent ester carbonyl oxygen (aryloxy oxygen) will be labeled **Aα** and **Bα** (**Aα′** and **Bα′**). In boat conformations, there is a large gap between adjacent rings. Conformers of the **Aα′** and **Bα′** classes should have too large a distance between the phenolic hydroxyl group and the adjacent aryloxy oxygen to give strong HBs; conformers of the **Aα** and **Bα** classes benefit of two more atoms (>C═O) to fill the large gap between the adjacent rings and could be expected to give stronger HBs. As a further possibility for the boats **B**, an intramolecular O−H···O═C bond can be formed between the two facing upward-oriented aromatic rings, giving the subgroup of **Bβ** conformations. Rather than the single HB starting model used above (corresponding to the class **Aα′** of **3**), we have then populated the above five classes of conformers (**Aα**, **Bα**, **Aα′**, **Bα′**, **Bβ**) by leaving the six benzoyl groups not involved in the HB free to rotate; a (*P*) stereochemistry was arbitrarily chosen for the calculations (the energies and some geometric features of the low energy conformers are gathered in Table S3, minimum-energy conformers of each class are sketched in Figures S9–S13). The B3LYP/6-31G* calculations indicate a high energy for conformers of the **Aα′**, **Bα′**, and **Aα** classes, as compared to those of the **Bα** and **Bβ** classes, consistent with longer lengths of their HBs. Among **B** boats, HB formation with the adjacent carbonyl (class **Bα**) is preferred over that with the facing carbonyl (**Bβ**): in the lower energy 1 kcal mol^{-1} window, we have six **Bα** conformers and a single **Bβ** conformer. Thus, despite the large number of possibilities, few conformers seem relevant in the conformational analysis of **3**. Spurred by this simplification, we compared the experimental spectrum with DFT and ZINDO calculations performed on the lowest energy conformer **Bα-1** (Figure 5). It can be seen that, as happened for

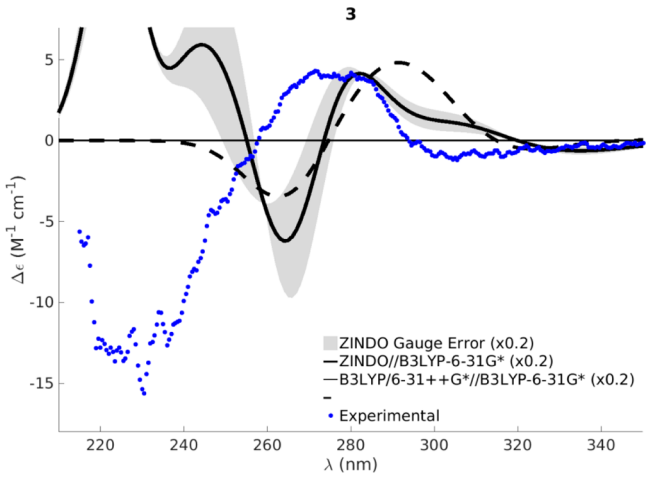

Figure 5. Comparison between the experimental ECD spectrum of the second-eluted fraction of **3** and the calculated ZINDO and B3LYP/6-31++G* spectra for the lowest energy conformer **Bα-1** of (*P*)-**3**. All computed spectra have been multiplied by a factor of 0.2. The continuous black line has been obtained as the average of the spectra obtained with the length and velocity formalism, which correspond to the upper and lower limits of the gray-shaded area.

the compounds considered above, also in this case the longer wavelength portion of the spectrum is reasonably paralleled by ECD computations on a single B3LYP/6-31G*-optimized conformer by either the B3LYP/6-31++G* or the much simpler ZINDO method. ZINDO calculations, on the other hand, qualitatively disagree at shorter wavelengths, where in the cases studied above the role of conformations was more important. Two further checks on the role of conformations have been performed. First, considering the good performances of the ZINDO method experienced above, we have computed the Boltzmann average of the ECD spectra at the ZINDO//B3LYP/6-31G* level, confirming the qualitative agreement at longer wavelengths and reducing significantly the computed positive peak at shorter wavelengths (Figure S14). Second, as in a boat conformation, the pendant groups on the methine bridges are rather close to the substituents of the two flattened rings A and D, and it can be argued that the relative orientation of the chromophores and then the spectrum could change as a result of that interaction, we checked this possibility by ZINDO computations on the 16 low energy conformers obtained for ethyl substituents starting from the lowest energy conformer **Bα-1**. Also in this case, the qualitative trend at longer wavelengths is unchanged (Figure S14).

DOI: 10.1021/acs.joc.6b02349
J. Org. Chem. 2017, 82, 202−210

According to the favorable comparison of the computed and the experimental spectrum, the AC of the (*P*)-isomer of **3** (Scheme 1) is then assigned to the second-eluted enantiomeric fraction (Figure 2). A summary of the AC assignments for the enantiomers of the resorcin[4]arenes under investigation is given in Table 3.

Table 3. AC Assignments to the Enantiomeric Fractions of Resorcin[4]arenes and Elution Order under the Optimized eHPLC Conditions Shown in Table 1[a]

	first-eluted	second-eluted
1a	(*P*); (1*S*,2*S*,3*S*,4*S*)	(*M*); (1*R*,2*R*,3*R*,4*R*)
1b	(*P*); (1*S*,2*S*,3*S*,4*S*)	(*M*); (1*R*,2*R*,3*R*,4*R*)
2a	(*P*); (1*S*,2*S*,3*S*,4*R*)	(*M*); (1*R*,2*R*,3*R*,4*S*)
2b	(*M*); (1*R*,2*R*,3*R*,4*S*)	(*P*); (1*S*,2*S*,3*S*,4*R*)
3	(*M*); (1*R*,2*S*,3*S*,4*R*)	(*P*); (1*S*,2*R*,3*R*,4*S*)

[a]The stereochemical notation refers to the atom numbering shown in Scheme 1.

In addition to the AC assignment of the compounds investigated here, it would be desirable to model the results in order to confidently assign the AC of similar compounds without recourse to full ab initio calculations. The saturated methine bridges render resorcin[4]arenes good candidates for the application of an excitonic model, whereby strong dipole-allowed transitions on molecular fragments are used to predict the signs of the ECD peaks. Indeed, the ECM has been considered in previous investigations on resorcin[4]-arenes.[23b,24]

The ECM is widely applied in the case of two equal chromophores 1 and 2, where it leads to the exciton chirality rule, stating that the sign of the couplet is determined by the sign of the dihedral angle defined by the two transition dipole vectors $\boldsymbol{\mu}_1$ and $\boldsymbol{\mu}_2$ placed at the extrema of a vector starting at 1 and ending at 2.[26] General formulas for more than two equal chromophores have also been reported.[26] However, as far as we know, explicit forms of those formulas in terms of the orientations of the transition dipoles within the excitonic fragments have only been worked out for C_3 symmetry.[27] Spurred by the ECD spectra of the C_4-symmetric **1a**,**b**, we have generalized the C_3 results reported in ref 27 to axes of order $n > 3$. The original model has been proposed for C_3-cyclotriveratrylene, where three aromatic rings have their long axes perpendicular to the C_3 axis.[27] In crown C_4-resorcin[4]arenes it is the short axis of the aromatic rings that is perpendicular to the C_4 axis. The model can easily cope with this change, but the restriction remains of an aromatic ring with one of its (either short or long) axes perpendicular to the C_4 symmetry axis. This essentially amounts to assuming a C_{nv} symmetry for the aromatic rings and considers that the loss of the vertical symmetry planes is only due to the substituents; therefore, this restriction rules out systems characterized by significant tilt angles.[19b] The theoretical analysis, detailed in the appendix, shows that for $n \geq 3$ equal aromatic rings arranged in C_n symmetry, one can anticipate the occurrence of ECD absorptions to three states A, E^+, and E^- (two forming a degenerate pair) with rotatory strengths

$$R^{(A)} = -\frac{R^{(E^{\pm})}}{2} = \frac{n\pi}{4\sin(\pi/n)} d_{12}\tilde{\nu}D\cos\Phi\sin 2\theta \quad (1)$$

where $\tilde{\nu}$ is the frequency of the UV absorption with dipolar strength $D = \mu^2$, where μ is the transition dipole moment, d_{12} is the distance of the centers of charge of two consecutive chromophores, Φ_i is the inclination angle of the *i*th ring (see Computational Methods), and θ is the angle of rotation of the transition dipole vector from the long axis HC−CH of the *i*th aromatic ring (Figure 6). As soon as the geometric scaffold of

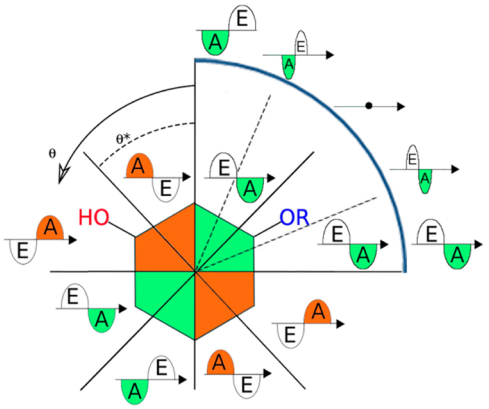

Figure 6. 4 × 2 = 8 sectors expected for the exciton chirality model applied to C_n-symmetric resorcin[4]arenes. Orange and green zones indicate positive and negative A peaks, respectively. The angle θ of the transition dipole vector is measured anticlockwise from the long axis of the aromatic ring toward the OH substituent. This amounts to an anticlockwise measurement from the *endo* side of the resorcin[4]-arenes studied of *M* stereochemistry.

the resorcin[4]arene is given, the angle Φ is a constant, while the angle θ depends on the electronic transition of the chromophore. As a final requirement to predict the sign of the couplet, in addition to eq 1, the relative energy of the excited states *A* and *E* should be stated. In the ECM, originally conceived for weakly interacting apolar fragments, the energy of those states is obtained considering an induced-dipole−induced-dipole interaction, where the induced dipoles are the electric transition dipole moments. This function is only weakly dependent upon the angle Φ and the number of chromophores *n* and changes sign close to $\theta^* \approx 45°$ (Figure S13). Therefore, for $\theta < \theta^*$ the interaction is repulsive and the in-phase state A has higher energy, while for $\theta > \theta^*$ the interaction is attractive and the in-phase state A has lower energy. This leads to the rule sketched in Figure 6 for the appearance of the exciton-induced couplet, which can be recognized as an adapted form of that reported for cycloveratrylene.[27,28]

In brief, the above theoretical discussion suggests a way to interpret the sign of the exciton-induced couplets considering only the direction of the dipole transition vector of the isolated chromophore; this direction can be obtained either from experiments or by calculations on a smaller fragment of the target molecule. To check the consistency of this prediction, we have computed the TDDFT B3LYP/6-31++G* spectra of minimum energy conformers of compounds **4a** (3-methoxyphenol) and **4b** (3-benzoxyphenol), which constitute a model for the resorcinol rings of **1a** and **1b**, respectively. Angles θ measured anticlockwise from the long axis in the direction of the OH group for the strongest UV transitions at longer wavelength are reported in Table 4. The character of the transitions reveals that they mainly concern the aromatic ring bearing the two substituents, as can be inferred from the sketches of molecular orbitals reported in the Supporting

DOI: 10.1021/acs.joc.6b02349
J. Org. Chem. 2017, 82, 202−210

Table 4. Absorption Wavelengths, Dipolar Strengths $D = \mu^2$, Anti-Clockwise Rotation θ of the Dipole Vector μ with Respect to Long Axes of the Aromatic Rings and Main Character of the Strongest Transitions for Compounds 4a and 4b in the Long-Wavelength Region

	state	λ (nm)	D (au)	θ (deg)	character
4a	2	247	0.049	−85	HOMO → LUMO+1
	6	219	0.104	−9	HOMO → LUMO+3
4b	3	250	0.461	−65	HOMO → LUMO+1
	10	221	0.508	−46	HOMO−1 → LUMO+1
	11	219	0.333	−7	HOMO → LUMO+5

Information (Table S4). The one significant exception is the state 10 of **4b**, which involves the pendant aromatic group. For the lowest energy conformation of **4b** the orientation of the transition dipole vector is close to the value where the ECM predicts a zero answer for the crossover of the A and E peaks (Figure 6), thus a vanishing ECD signal. However, this fortunate coincidence will not hold for other conformations of **4b**, and thus, the significant conformational dependence of the spectra of **1b** and **2b** reported in Figure 4 is qualitatively understandable in terms of the ECM.

The spectral region studied here stems from electronic transition of chromophores corresponding to the forbidden B_{2u} and B_{1u} transitions of benzene (260 and 210 nm), which are polarized in-plane along its short and long axis, respectively. According to Platt's nomenclature,[21] these transitions are called ^1L_b and ^1L_a, and this nomenclature is often preferred over the standard Mulliken one, as it depends on azimuthal node counting of orbitals, a feature which is generally preserved upon loss of symmetry. Previous studies on resorcin[4]arenes have been focused on the ^1L_b transitions. Nicely enough, we see that the low energy negative couplets for (*M*)-**1a** and (*M*)-**1b**, those derived by the ^1L_b transitions, are consistent with the signs of the angles θ (−85° and −65°) computed for the isolated rings **4a** and **4b** in their lowest energy conformation. The fact that the low energy couplet is similar in (*M*)-**2a** and (*M*)-**2b**, though of smaller magnitude, can then be qualitatively interpreted considering that each resorcinol contributes to the couplet according to its axial chirality *M* or *P*.

In contrast to the positive finding regarding the ^1L_b transitions, which confirms and extends the results of previous investigations,[24] we note that the sign of the couplets predictable from the orientation of the ^1L_a-derived transitions is opposite to the sign of the higher energy couplet in the ECD spectra of **1a,b**. In an attempt to understand this failure, we have investigated the nature of the strongest ECD transitions in the TDDFT calculations on **1a** and **1b** (Tables S3 and S4). For **1a**, the strongest transitions at longer wavelength involve the aromatic rings of the resorcin[4]arene. However, the transitions at shorter wavelengths involve excited orbitals with a significant contribution from σ^*(CH) orbitals and oxygen lone pairs, thus not conforming to the assumptions of the ECM. For **1b**, the computed spectrum has many contributions from excited states generated from virtual orbitals, which are localized on the pendant aromatic rings. These contributions are dominant in the shorter wavelength portion of the spectrum. Thus, a simplified model with excitons only on the aromatic ring forming the calix is inadequate at shorter wavelengths. The ^1L_a-derived transitions then require a model with a larger active space.

Conclusions. The use of resorcin[4]arenes for chiral recognition processes could benefit from the possibility of designing chiral bowls by suitable substitution patterns on the upper rim. Indeed, a rather large set of these molecules has been effectively synthesized. Their use requires the assessment of their stereochemistry, which, with some notable exceptions based on diffraction studies,[29] is often unknown. Here we have determined the AC of five chiral resorcin[4]arenes by comparison of experimental ECD spectra, as measured by application of the stopped-flow eHPLC−CD technique, with DFT and semiempirical calculations. In addition to the full calculations, we have also applied the exciton chirality model (ECM), and we have seen that it is effective in predicting the first couplet at longer wavelength. This model, here generalized to C_n symmetry, could be used in further AC determinations, when considering the long wavelength side, but, at least in its simplest form, it should not be used for the couplet at shorter wavelengths, which are significantly affected by other states not considered in the ECM.

EXPERIMENTAL SECTION

Synthesis. All compounds have been synthesized according to ref 13.

Stopped-Flow eHPLC−CD Analysis. The enantioseparation of all racemic mixtures was performed on an HPLC system equipped with a 20 μL sample injection loop, and the optimization of chromatographic conditions was carried out using different eHPLC columns with polysaccharide-based chiral stationary phases, mobile-phase compositions, and flow rates; all separations were carried out in normal-phase conditions at a controlled temperature of 15 °C and a detection wavelength of 230 nm. Lux Cellulose-1 (cellulose tris(3,5-dimethylphenylcarbamate), 3 μm, 250 × 4.6 mm i.d.), Lux Cellulose-2 (cellulose tris(3-chloro-4-methylphenylcarbamate), 3 μm, 250 × 4.6 mm i.d.), Lux Cellulose-3 (cellulose tris(4-methylbenzoate), 3 μm, 250 × 4.6 mm i.d.), Lux Cellulose-4 (cellulose tris(4-chloro-3-methylphenylcarbamate), 3 μm, 250 × 4.6 mm i.d.), and Lux Amylose-2 (amylose tris(5-chloro-2-methylphenylcarbamate), 3 μm, 250 × 4.6 mm i.d.) were purchased from Phenomenex (Castel Maggiore, Italy). Chiralcel OJ (cellulose tris(4-methylbenzoate), 10 μm, 250 × 4.6 mm i.d.), Chiralpak AD (amylose tris(3,5-dimethylphenylcarbamate), 10 μm, 250 × 4.6 mm i.d.), and Chiralcel OD-H (cellulose tris(3,5-dimethylphenylcarbamate), 5 μm, 250 × 4.6 mm i.d.) were purchased from Daicel (Chiral Technologies Europe, Illkirch, France). Methanol (99.9%), 2-propanol (99.9%) and *n*-hexane (97%) were HPLC-grade.

The spectroscopic analysis was performed under optimized chromatographic conditions using the stopped-flow eHPLC−CD technique. The setup of the HPLC system was modified: the 20 μL injection loop was replaced with a 100 μL loop to increase the loading, and a spectropolarimeter equipped with a 10 mm path length HPLC flow cell was connected to the system as an additional detector; a three-way was mounted between the HPLC system and the spectropolarimeter for stopped-flow measurements. The enantiomeric fractions were stopped inside the HPLC flow cell during their elution and analyzed by full-spectrum ECD spectroscopy in the 350−215 nm spectral range, using a 4 nm spectral bandwidth, a 50 nm min^{-1} scanning speed, a 1 s data integration time, a 0.2 nm data pitch, and three accumulation cycles. Stopped-flow spectra were blank-corrected using stopped-flow measurements of the mobile phase under the same conditions, which were repeated before and after each measurement on the fractions in order to correct baseline drifts. Each enantiomeric fraction was analyzed three times according to this protocol; the resulting stopped-flow spectra were normalized at the maximum of the lowest energy absorption band in order to account for the different instantaneous concentrations inside the HPLC flow cell and converted in molar units based on the molar extinction coefficient of the racemic mixture.

DOI: 10.1021/acs.joc.6b02349
J. Org. Chem. 2017, 82, 202−210

Computational Methods. In order to simplify computations, undecyl chains have been always substituted by methyl groups. The chirality was arbitrarily chosen as (*M*) for the 4 tetra-*O*-substituted resorcin[4]arenes and (*P*) for **3**. Preliminary conformational searches have been performed at the Merck Force Field level (MMFF)[30] by Spartan 02.[31] Ab initio computations have been performed with Gaussian 09;[32] TDDFT calculations have been performed considering 50 excited states; spectra have been computed without frequency shifts and using a Gaussian profile for peak shapes with standard deviation σ = 0.17 eV. Inspection of molecular orbitals and preparation of their sketches (Tables S4−S6) have been performed with Avogadro.[33] For the tetra-*O*-substituted resorcin[4]arenes (**1a**, **1b**, **2a**, and **2b**), the ECD spectra have been first computed for a single C_4-symmetric conformer at the B3LYP/6-31++G*//6-31G* level. The effect of different conformations of the substituents was then investigated at the semiempirical ZINDO level for **1b** and **2b**. For the hepta-*O*-substituted resorcin[4]arene **3**, five independent conformational searches were performed by SPARTAN, constraining a single distance in order to have structures with well-defined HBs between the phenol hydroxyl group and the ester carbonyl group of the adjacent ring (classes **A**α and **B**α), between the phenol hydroxyl group and the ester carbonyl group of the facing ring (class **B**β), and between the phenol hydroxyl group and the adjacent ester aryloxy group (classes **A**α' and **B**α'). These MMFF-constrained structures were then fully optimized at the B3LYP/6-31G* level. Low energy conformers of each class are gathered in Table S3. The ECD spectra of these conformers have been computed by Gaussian at the ZINDO level. The ECD spectrum of the lowest energy conformer **B**α**-1** has also been computed at the TDDFT B3LYP/6-31++G* level.

The inclination angle Φ_i has been computed as the excess over 90° of the valence angle α(X-C′$_i$-C″$_i$), where C′$_i$ and C″$_i$ are the C atoms of the aromatic methines of the *i*-th ring contained in the lower and in the upper rim, respectively, and X is a dummy atom located in the center of mass of the 4 C′ atoms.

■ ASSOCIATED CONTENT

Supporting Information

The Supporting Information is available free of charge on the ACS Publications website at DOI: 10.1021/acs.joc.6b02349.

Tables of chromatographic parameters obtained during the optimization of the eHPLC analysis, experimental UV and ECD spectra, relative energies of conformers of **3**, sketches of relevant molecular orbitals for **1a**, **1b**, **4a**, and **4b**, sketches of minimum-energy selected structures, detailed derivation of eq 1 for the exciton chirality model applied to systems of C_n symmetry, dependence of the critical angle upon the order of the axis and the twist angle Φ (PDF)

■ AUTHOR INFORMATION

Corresponding Authors

*E-mail: neri@unisa.it.
*E-mail: gmonaco@unisa.it.
*E-mail: daniele.tedesco@unibo.it.

ORCID

Guglielmo Monaco: 0000-0001-5268-940X

Notes

The authors declare no competing financial interest.

■ ACKNOWLEDGMENTS

Financial support from MIUR (FARB 2013 of the University of Salerno, University of Bologna) is gratefully acknowledged. The HPLC flow cell for online ECD analyses was kindly provided by the research group of Prof. Stefano Masiero (Department of Chemistry, University of Bologna).

■ REFERENCES

(1) (a) Neri, P., Sessler, J. L., Wang, M.-X., Eds. *Calixarenes and Beyond*; Springer: Switzerland, 2016. (b) Rissanen, K. *Angew. Chem., Int. Ed.* **2005**, *44*, 3652−3654.

(2) *Container Molecules and Their Guests*; Royal Society of Chemistry: Cambridge, 1997.

(3) (a) Pochorovski, I.; Diederich, F. *Acc. Chem. Res.* **2014**, *47*, 2096−105. (b) Purse, B. W.; Rebek, J., Jr. *Proc. Natl. Acad. Sci. U. S. A.* **2005**, *102*, 10777−10782.

(4) For recent reviews, see: (a) Ajami, D.; Liu, L.; Rebek, J., Jr. *Chem. Soc. Rev.* **2015**, *44*, 490−499. (b) Ajami, D.; Rebek, J., Jr. *Acc. Chem. Res.* **2013**, *46*, 990−999. (c) Avram, L.; Cohen, Y.; Rebek, J., Jr. *Chem. Commun.* **2011**, *47*, 5386−5375.

(5) McIldowie, M. J.; Mocerino, M.; Ogden, M. I. *Supramol. Chem.* **2010**, *22*, 13−39.

(6) Dalla Cort, A.; Mandolini, L.; Pasquini, C.; Schiaffino, L. *New J. Chem.* **2004**, *28*, 1198−1199.

(7) Szumna, A. *Chem. Soc. Rev.* **2010**, *39*, 4274−4285.

(8) (a) Jedrzejewska, H.; Kwit, M.; Szumna, A. *Chem. Commun.* **2015**, *51*, 13799−13801. (b) Jedrzejewska, H.; Wierzbicki, M.; Cmoch, P.; Rissanen, K.; Szumna, A. *Angew. Chem., Int. Ed.* **2014**, *53*, 13760−13764.

(9) Autschbach, J. *Chirality* **2009**, *21*, E116−E152.

(10) *Comprehensive Chiroptical Spectroscopy*; Berova, N., Ed.; Wiley: Hoboken, 2012.

(11) Troisi, F.; Pierro, T.; Gaeta, C.; Carratù, M.; Neri, P. *Tetrahedron Lett.* **2009**, *50*, 4416−4419.

(12) Talotta, C.; Gaeta, C.; Troisi, F.; Monaco, G.; Zanasi, R.; Mazzeo, G.; Rosini, C.; Neri, P. *Org. Lett.* **2010**, *12*, 2912−2915.

(13) Farina, F.; Talotta, C.; Gaeta, C.; Neri, P. *Org. Lett.* **2011**, *13*, 4842−4845.

(14) Bertucci, C.; Tedesco, D. *J. Chromatogr. A* **2012**, *1269*, 69−81.

(15) Tedesco, D.; Fabini, E.; Barbakadze, V.; Merlani, M.; Zanasi, R.; Chankvetadze, B.; Bertucci, C. *Chirality* **2015**, *27*, 914−918.

(16) Helmchen, G., Herrmann, R., Houben, J., Müller, E., Weyl, T., Büchel, K. H., Eds. *Methods of Organic Chemistry. E Vol. E 21 F: Additional and Supplementary Volumes to the 4th ed. Stereoselective Synthesis*; Thieme, Stuttgart, 1996.

(17) Buckley, B. R.; Boxhall, J. Y.; Bulman Page, P. C.; Chan, Y.; Elsegood, M. R. J.; Heaney, H.; Holmes, K. E.; McIldowie, M. J.; McKee, V.; McGrath, M. J.; Mocerino, M.; Poulton, A. M.; Sampler, E. P.; Skelton, B. W.; White, A. H. *Eur. J. Org. Chem.* **2006**, *2006*, 5117−5134.

(18) Mäkinen, M.; Jalkanen, J.-P.; Vainiotalo, P. *Tetrahedron* **2002**, *58*, 8591−8596.

(19) (a) Nissinen, M.; Wegelius, E.; Falábu, D.; Rissanen, K. *CrystEngComm* **2000**, *2*, 151−153. (b) Salorinne, K.; Nissinen, M. *CrystEngComm* **2009**, *11*, 1572.

(20) Ugozzoli, F.; Andreetti, G. D. *J. Inclusion Phenom. Mol. Recognit. Chem.* **1992**, *13*, 337−348.

(21) Platt, J. R. *J. Chem. Phys.* **1949**, *17*, 484.

(22) Warnke, I.; Furche, F. *Wiley Interdiscip. Rev. Comput. Mol. Sci.* **2012**, *2*, 150−166.

(23) (a) Klaes, M.; Neumann, B.; Stammler, H.-G.; Mattay, J. *Eur. J. Org. Chem.* **2005**, *2005*, 864−868. (b) Schiel, C.; Hembury, G. A.; Borovkov, V. V.; Klaes, M.; Agena, C.; Wada, T.; Grimme, S.; Inoue, Y.; Mattay, J. *J. Org. Chem.* **2006**, *71*, 976−982.

(24) Kuberski, B.; Pecul, M.; Szumna, A. *Eur. J. Org. Chem.* **2008**, *2008*, 3069−3078.

(25) Da Motta Neto, J. D.; Zerner, M. C. *Int. J. Quantum Chem.* **2001**, *81*, 187−201.

(26) Harada, N.; Nakanishi, K.; Berova, N. In *Comprehensive Chiroptical Spectroscopy*; Berova, N., Polavarapu, P. L., Nakanishi, K., Woody, R. W., Eds.; John Wiley & Sons: Hoboken, 2012; pp 115−166.

(27) Canceill, J.; Collet, A.; Gabard, J.; Gottarelli, G.; Spada, G. P. *J. Am. Chem. Soc.* **1985**, *107*, 1299−1308.

DOI: 10.1021/acs.joc.6b02349
J. Org. Chem. 2017, 82, 202−210

(28) Andraud, C.; Garcia, C.; Collet, A. In *Circular Dichroism*; Berova, N., Nakanishi, K., Eds.; John Wiley & Sons, Inc.: New York, 2000; pp 115−166.
(29) Buckley, B. R.; Page, P. C. B.; Chan, Y.; Heaney, H.; Klaes, M.; McIldowie, M. J.; McKee, V.; Mattay, J.; Mocerino, M.; Moreno, E.; et al. *Eur. J. Org. Chem.* **2006**, *2006*, 5135−5151.
(30) Halgren, T. A. *J. Comput. Chem.* **1999**, *20*, 730−748.
(31) *Spartan 02*; Wavefunction, Inc.: Irvine, CA, 2002.
(32) Frisch, M. J. *Gaussian 09*, Revision D.01; Gaussian, Inc.: Wallingford, CT, 2013.
(33) *Avogadro: an open-source molecular builder and visualization tool*, Version 1.0.1; http://avogadro.openmolecules.net/.

DOI: 10.1021/acs.joc.6b02349
J. Org. Chem. 2017, 82, 202−210